JPEDAV (2007) 28:523–535
DOI: 10.1007/s11669-007-9203-x
1547-7037 ©ASM International

Experimental Investigation and Thermodynamic Calculation of Mg-Al-Sn Phase Equilibria and Solidification Microstructures

E. Doernberg, A. Kozlov, and R. Schmid-Fetzer

(Submitted October 27, 2006; in revised form May 25, 2007)

Experimental work using differential scanning calorimetry, differential thermal analysis, X-ray diffraction, scanning electron microscopy, and energy-dispersive X-ray analysis was conducted on key samples with more than 33 at.% Mg in the Mg-Al-Sn system. In addition to the thermal analysis and study of the solidification microstructure, an equilibration at 400 °C was performed. The results were used together with all available phase equilibria and thermodynamic data from earlier experimentation to create a consistent thermodynamic description of the Mg-Al-Sn alloy system. No ternary stable phase was discovered, and no ternary solubilities of the binary intermetallic phases were found. With the addition of a single Gibbs energy parameter describing the interaction between Al and the associate Mg_2Sn in the liquid phase, the thermodynamic model of the system could be made to describe all pertinent experimental data throughout the ternary system. The phase precipitation sequence during slow solidification of all present samples is reflected by the thermodynamic calculations as well. Intricate details of the liquid miscibility gap, occurring in ternary alloys only, are also highlighted.

Keywords CALPHAD, experimental phase equilibria, liquidus surface, microstructure, ternary phase diagram, thermodynamic assessment

1. Introduction

For magnesium to compete successfully with aluminum on the market for lightweight engineering metals, the knowledge gaps must be closed in as many alloying systems as possible. The alloying elements aluminum and tin improve the castability of magnesium by reducing the melting point, with the advantage that the overall alloy strength is not compromised. It will not necessarily be the simple ternary system of Mg-Al-Sn that marks the way of the future for magnesium alloys, but more complex multicomponent systems also containing these elements. To model quaternary and higher-order systems, it is vital that the underlying ternary phase diagrams be based on sound experimental research and correct thermodynamic modeling.

The previous research conducted on the binary systems is considered to be sound. Assessment of the Al-Sn system is taken from Fries and Lukas,[1] the Mg-Sn system is taken from Fries and Lukas[2] with a subsequent correction by Fries,[3] and the Al-Mg system is taken from Liang et al.[4] The crystallographic data for the stable binary phases are given in Table 1. A number of authors, listed in Table 2, have also conducted metallographic, thermodynamic, and phase equilibria investigations in the ternary Mg-Al-Sn system whereby the (Mg)-Mg_2Sn-γ triangle has been the main point of focus. No ternary solubilities of the binary phases listed in Table 1, and no stable ternary phases have been reported. Reviews of the system have been written by Raynor[5] and Rokhlin and Lukas,[6] considering literature up to and including work by Sommer et al.[7] in Table 2.

Although a number of authors have published phase diagrams and sections of the liquidus surface, all are based on graphical evaluation of experimental data, rather than thermodynamic modeling. Thermodynamic calculations have been used to model the measured mixing enthalpy in the ternary system;[7] however, no Calphad-type assessment was made to prove the consistency of this model with respect to phase equilibria.

The principle objective of this study is to present a consistent thermodynamic description of the Mg-Al-Sn alloy system. Key samples are chosen to detect any possible ternary solubility of the known binary compounds and to investigate the phase equilibria by also analyzing the exact solidification sequence. Original experimental data[8-10] along with the thermal analysis results from the samples chosen for the current study are used to refine the thermodynamic model of the system. The starting point for optimization was a calculation of the phase equilibria by extrapolation from the binary edge systems that also served as a selection of the key samples. Powder x-ray diffraction (XRD) experiments and metallographic investigation with a scanning electron microscope (SEM) using energy-dispersive x-ray analysis (EDX) are presented to prove the consistency of the calculated phase equilibria. Further

E. Doernberg, A. Kozlov, and **R. Schmid-Fetzer,** Institute of Metallurgy, Clausthal University of Technology, Robert-Koch-Str. 42, D-38678 Clausthal-Zellerfeld, Germany. Contact: e-mail: schmid-fetzer@tu-clausthal.de

Table 1 Crystallographic data of solid phases in the binary edge systems

Phase/temperature range in °C	Pearson symbol	Space group	Lattice parameters, pm	Solubility range	Ref
(Al) < 660.425	*cF*4	$Fm\bar{3}m$	a = 404.88	Pure Al	19
(Mg) < 650	*hP*2	$P6_3/mmc$	a = 320.89, c = 521.01	Pure Mg	19
Sn (white/β) 231.968-13	*tI*4	$I4_1/amd$	a = 583.18, c = 318.18	Pure Sn	19
αSn (gray) < 13	*cF*8	$Fd\bar{3}m$	a = 648.92	Pure Sn	19
β-Mg_2Al_3 < 452	*cF*1168	$Fd\bar{3}m$	a = 2816-2824	60-62 at.% Al	6
γ-$Mg_{17}Al_{12}$ < 458	*cI*58	$I\bar{4}3m$	a = 1054.38	39.5-51.5 at.% Al	6
ε-$Mg_{23}Al_{30}$ 410-250	*hR*159	$R\bar{3}$	a = 1282.54, c = 2174.78	54.5-56.5 at.% Al	6
Mg_2Sn < 770	*cF*12	$Fm\bar{3}m$	a = 676.5		13

Table 2 Previous investigations of the Mg-Al-Sn phase equilibria

Reference	Method/Experimental technique	Phase range or composition range, at.%
Hume-Rothery et al.[20]	Microscopic analysis + electron concentration measurements	Mg65Sn32Al3
Westlinning and Klemm[21]	X-ray and microscopic analyses	Solubility of Mg_2Sn in solid (Al)
DowChemicals[8]	X-ray diffraction, optical metallography	γ-$Mg_{17}Al_{12}$ - Mg_2Sn (11 evenly spaced samples)
Badaeva and Kusnetsova[9]	Thermal + microscopic analyses	9 vertical sections Al - Mg_xSn_{x-1}; Mg_2Sn - β-Mg_2Al_3
Kopetsky and Semenova[22]	Thermal + microscopic analyses, electrical conductivity	γ-$Mg_{17}Al_{12}$ - Mg_2Sn - Mg; Mg94Sn6 - Mg77Al23
Semenova[10]	Thermal + microscopic analyses	Mg_2Sn - γ-$Mg_{17}Al_{12}$; Mg85Al15 - Al15Sn85; Mg85Sn15 - Al85Sn15
Semenova[23]	Thermal + microscopic analyses, x-ray diffraction	γ-$Mg_{17}Al_{12}$ - Mg_2Sn - Mg
Sommer et al.[7]	Mixing calorimetry (liquid)	835 °C; 735 °C/Mg_2Sn - Al; Mg30Sn7 - Al; Mg50Sn5 - Al; Al50Sn50 - Sn
Bowles et al.[24]	Optical microscopy, SEM, XRD. Vickers macrohardness	Mg99Sn1, Mg95Sn5, Mg88Sn5Al7, Mg83Sn10Al7, Mg78Sn15Al7, Mg56.6Sn36.4Al7

comparisons are made using the enthalpy data of Sommer et al.[7]

2. Experimental Procedures

2.1 Sample Preparation

The key sample compositions shown in Fig. 1 were chosen to complement the results found in the literature and are focused on the magnesium-rich part of the system. The exact sample compositions can be seen in Table 3. For each composition, two samples were prepared. The first was used for thermal analysis and later for microstructural analysis, while the second was annealed at 400 °C for 3 weeks in order for the sample to reach a state of equilibrium and was then used for x-ray powder diffraction.

The starting materials were Mg pieces (99.98 mass%), Al ingot (99.999 mass%), and Sn bar (99.999 mass%) all from Alfa Aesar GmbH & Co KG, Karlsruhe, Germany. The pure elements were weighed, pressed into pellets to break any oxide layers, and placed in a thin-walled tantalum (Ta) capsule that comprised of a small cylinder and two ends. The second end was arc welded onto the filled capsule under a 1 bar argon atmosphere. This reduces the possibility of sample contamination, oxidation, or loss due to vaporization, which makes possible[11] repeated heating and cooling cycles during testing. All samples were melted in an evacuated test oven to allow alloy formation to take place

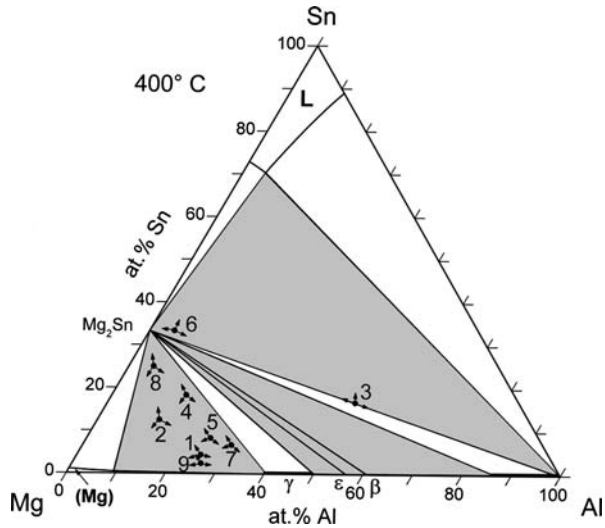

Fig. 1 Calculated isothermal section of the Mg-Al-Sn phase diagram at 400 °C; the dots represent the sample compositions investigated in this study; arrows point to the identified phases. Three phase regions are shown in gray

Table 3 Temperatures extracted from the DSC (samples 1-3) and DTA (samples 4-9) curves and their interpretation. Invariant reactions were recognized from the peak shape

No.	Sample composition in at.%	Thermal signals			Interpretation	
		Heating(a), °C	Cooling(b), °C	Evaluation temperature, °C	Calculation temperature,°C	Phase boundary or invariant reaction
1	70.6 Mg	···	···	>500(c)	536	L/L + Mg_2Sn
	25.0 Al	439	436	439	447	L + Mg_2Sn/L + Mg_2Sn + (Mg)
	4.4 Sn	434	433	434	431	**E_4: L ↔ Mg_2Sn + γ-$Mg_{17}Al_{12}$ + (Mg)**
2	75.0 Mg	629	634	632	632	L/L + Mg_2Sn
	12.5 Al	489w	490w	490	496	L + Mg_2Sn/L + Mg_2Sn + (Mg)
	12.5 Sn	433	432	433	431	**E_4: L ↔ Mg_2Sn + γ-$Mg_{17}Al_{12}$ + (Mg)**
3	33.3 Mg	678	676	677	695	L′/L′ + Mg_2Sn
	50.0 Al	611	610	611	606	L′ + Mg_2Sn/L′ + Mg_2Sn + (Al)
	16.7 Sn	607w	606w	607	602	**E_1: L′ ↔ L″ + Mg_2Sn + (Al)**
		n.d.	n.d.	···	202	**E_5: L ↔ Mg_2Sn + (Al) + Sn**
4	66.7 Mg	699	700	700	708	L/L + Mg_2Sn
	15.0 Al	440w	438w	439	438	L + Mg_2Sn / L + Mg_2Sn + γ-$Mg_{17}Al_{12}$
	18.3 Sn	429	428	429	431	**E_4: L ↔ Mg_2Sn + γ-$Mg_{17}Al_{12}$ + (Mg)**
5	66.7 Mg	n.d.	621	621	619	L/L + Mg_2Sn
	25.0 Al	442w	435w	437	440	L + Mg_2Sn/L + Mg_2Sn + γ-$Mg_{17}Al_{12}$
	8.3 Sn	431	430	431	431	**E_4: L ↔ Mg_2Sn + γ-$Mg_{17}Al_{12}$ + (Mg)**
6	61.7 Mg	759	749	754	754	L/L + Mg_2Sn
	5.0 Al	n.d.	n.d.	···	673	L + Mg_2Sn/L′ + L″ + Mg_2Sn
	33.3 Sn	n.d.	n.d.	···	602	**E_1: L′ ↔ L″ + Mg_2Sn + (Al)**
		201w	187w	200	202	**E_5: L ↔ Mg_2Sn + (Al) + Sn**
7	63.3 Mg	651	613	614	607	L/L + Mg_2Sn
	30.0 Al	449w	448w	449	449	L + Mg_2Sn/L + Mg_2Sn + γ-$Mg_{17}Al_{12}$
	6.7 Sn	430	427	429	431	**E_4: L ↔ Mg_2Sn + γ-$Mg_{17}Al_{12}$ + (Mg)**
8	70.0 Mg	739	738	739	737	L/L + Mg_2Sn
	5.0 Al	491w	489w	490	496	L + Mg_2Sn/L + Mg_2Sn + (Mg)
	25.0 Sn	432	428	430	431	**E_4: L ↔ Mg_2Sn + γ-$Mg_{17}Al_{12}$ + (Mg)**
9	26.0 Mg	483w	491w	490	478	L/L + Mg_2Sn
	71.6 Al	437w	438w	438	449	L + Mg_2Sn/L + Mg_2Sn + (Mg)
	2.4 Sn	429	426	428	431	**E_4: L ↔ Mg_2Sn + γ-$Mg_{17}Al_{12}$ + (Mg)**

(a) Onset for invariant reactions, peak maximum otherwise. (b) Onset. (c) Maximum temperature of heating cycle for sample 1. w, weak and diffuse signal; n.d., not detected

and to check if the weld on the Ta capsule was secure before performing the DSC/DTA-SEM/EDX experiments (first sample) and the annealing-XRD experiments (second sample), as detailed below.

2.2 DSC/DTA

Thermal analyses by differential scanning calorimetry (DSC) were performed on samples 1 to 3 using a Setaram MHTC 96 DSC apparatus (SETARAM Instrumentation, Caluire, France). Differential thermal analyses (Netzsch DTA 404 S, NETZSCH-Gerätebau GmbH, Selb, Germany) were used to locate the thermal signals corresponding to the liquidus temperature and invariant reactions of samples 4 to 9. For all samples, tests were run at ±5 K/min from about 50 K below to about 50 K above the expected reaction temperature. Using results from previous authors and calculated phase diagrams based on extrapolation from the binary systems, the following maximum testing temperatures were chosen: samples 1 and 4, 500 °C; samples 2, 3, 5, and 7, 700 °C; sample 6, 850 °C; and sample 9, 600 °C. Where the thermal peaks were very close together or difficult to define, samples were tested again at ±1 K/min in a temperature interval around the peaks. Each test included three heating and cooling cycles, where the first heating cycle usually did not show reasonable results. No reactions between the samples and the Ta capsule were observed. There were also no signs of reaction between the outside of the Ta capsule and sample holder or protective gas of the DSC/DTA apparatus.

2.3 XRD

The annealed samples were analyzed by powder x-ray diffraction using a Siemens D5000 diffractometer (Siemens, Germany). The samples were first ground with a mortar and pestle until they took on the form of a very fine powder. This was then placed in the middle of the groove in a plastic

sample holder and pressed flat and smooth with a piece of glass. Each sample was analyzed using Co Kα radiation in the range of $20° < 2\theta < 80°$ with a step size of 0.02° every 5 s. For the analysis of the diffractograms the software package Powder Cell[12] was used. The raw data were compared with calculated spectra based on crystallographic data[13] for each of the phases that were expected, and some of those that were not expected. By matching all the peaks in the diffractogram, the phases present in each sample could be identified. The relative amount of each phase was qualitatively determined.

2.4 SEM/EDX

A CamScan 44 scanning electron microscope (Obducat CamScan, Cambridge) (SEM) was used to analyze the microstructure of the samples after thermal analysis. Back-scattered electrons were used to make the images shown in this publication, while secondary electron images were used to help identify the difference between a darker phase and a depression or hole in the surface of the sample before conducting energy-dispersive x-ray (EDX) analysis.

For optimal resolution in the SEM, the samples were embedded in electrically conductive material and polished to 1 μm. A generous application of conductive tape proved helpful in reducing the development of static charges on the surface of the samples that reduce the possible resolution of the photos.

EDX analysis was conducted at a central position in large crystals (mostly above 5 μm) of each phase. Due to the depth of penetration of the electron beam and the excited volume, measurements on phases with a visible diameter of less than 5 μm could not be considered accurate. By considering the composition of the neighboring phase fields, an assumption could be made about which known phase was in question.

3. Experimental Results

The results of the thermal analysis of the nine samples investigated in this work are presented in Table 3. The values listed in the columns "Heating" and "Cooling" are already averages consisting of the results from two or more heat treatment cycles, whereby unrealistic results were previously discarded. For example, the liquidus temperature shown for sample 3 on heating (678 °C) consists of the following measurements: at 5 K/min: 677, 679, and 678 °C, and at 1 K/min: 675, 677, and 679 °C. The temperatures taken from the first cycle in each experiment were discarded because of the shape of the curve, and also previous experience has shown that the first heating cycle does not produce reliable values. The average of the remaining four experimental values gives the listed value of 678 °C. The values in the column headed "Evaluated Temperature" represents the experimentally suggested phase transition temperature from both the heating and cooling signals, giving less weight to the latter in the case of substantial supercooling. The interpretations of each thermal signal, including the assigned phase boundary or invariant reaction and the calculated temperatures, refer to the phase diagrams calculated using the thermodynamic model of the ternary system created during this investigation. The table is best read from right to left. All possible thermal signals, as predicted by the thermodynamic model of the system, are listed in the interpretation section. Some of these phase boundaries or invariant reactions were not detected during DSC or DTA experiments, for example E_5 in sample 3. Considering the very small amount of liquid that solidifies in sample 3 at E_5, which can be revealed by a separate thermodynamic calculation of phase fractions, it is not surprising that this reaction is not detectable. Although it may appear from the entries in Table 3, for samples 3 and 6, that a four-phase reaction (E_1) is followed by a four-phase reaction (E_5), the three-phase field $L'' + Mg_2Sn + (Al)$ is of course predicted between these two reactions. This can be seen in the corresponding *T-x* phase diagrams, which are shown later. This three-phase field is not shown in Table 3 since it cannot produce an additional thermal signal. From the entries in Table 3, it already becomes clear that the experimental data from the present study are in good agreement with the data calculated from the thermodynamic model.

The order of phase evolution during solidification is also confirmed by the microstructures of each sample in which the phase identification was based on local chemical composition determined by EDX analysis. The solubilities of Sn in γ-$Mg_{17}Al_{12}$ and of Al in Mg_2Sn were measured using EDX and were found to be insignificant. In the discussion section of this paper, a number of scanning electron micrographs serve as examples of typical microstructure development in the different sections of the Mg-Al-Sn system. The results of the XRD experiments conducted on the annealed samples also confirmed the phases present in each alloy and showed similar relative amounts of each phase. No peaks belonging to oxides or contaminations from the Ta capsule were detected, and no new peaks indicating a new ternary phase were observed. The peaks generated from the intermetallic phases γ-$Mg_{17}Al_{12}$ and Mg_2Sn were not shifted to the left or right of the 2θ positions calculated by Powder Cell[12] for the perfect crystals according to Table 1, which provided further confirmation that the ternary solubilities of these phases are insignificant. A summary of the results of phase analysis by both XRD and SEM/EDX is given individually for each sample by the arrows in Fig. 1.

4. Thermodynamic Modeling

The present modeling of the ternary phase equilibria is based on the published binary thermodynamic data sets of the subsystems Al-Sn,[1] Mg-Sn,[2] with a subsequent correction,[3] and Al-Mg.[4]

The Gibbs energy function $G_i^{0,j}(T) = G_i^j(T) - H_i^{SER}$ for the element i (i = Al, Mg, Sn) in the ϕ phase [ϕ = face-centered cubic, or fcc (Al, αSn), body-centered tetragonal,

or bct (βSn), close-packed hexagonal cph (Mg), liquid] is described by:

$$G_i^{0,j}(T) = a + b \cdot T + c \cdot T \cdot \ln T + d \cdot T^2 + e \cdot T^3 + f \cdot T^{-1} + g \cdot T^7 + h \cdot T^{-9} \quad \text{(Eq 1)}$$

where H_i^{SER} is the molar enthalpy of the stable element reference (SER) at 298.15 K and 1 bar, and T is the absolute temperature. The Gibbs energy functions for Al, Mg and Sn are taken from the SGTE compilation of Dinsdale.[14]

The Gibbs energy functions of all stoichiometric compounds (Mg_2Sn, β-Mg_2Al_3, ε-$Mg_{23}Al_{30}$) are described by the function:

$$G^{A_mB_n}(T) = \frac{m}{m+n} \cdot G_A^{0,\phi}(T) + \frac{n}{m+n} \cdot G_B^{0,\phi}(T) + a_{mn} + b_{mn} \cdot T \quad \text{(Eq 2)}$$

where a_{mn} and b_{mn} are parameters for the enthalpy of formation and the negative entropy of formation. The elemental component phases Sn (white/β) and αSn (gray) are also treated as pure stoichiometric phases. The γ-$Al_{12}Mg_{17}$ phase shows a binary solubility range and is modeled as a sublattice compound with three sublattices. As no ternary solubility has been detected, the thermodynamic description remains unchanged from the binary system.[4]

The fcc (Al), and cph (Mg) solution phases are described by the disordered substitutional solution model. For the phase ϕ, the molar Gibbs energy is expressed by:

$$G^{\phi}(T) = \sum_{i=1}^{3} x_i G_i^{0,\phi}(T) + RT \sum_{i=1}^{3} x_i \ln x_i + {}^{E}G^{bin,\phi} \quad \text{(Eq 3)}$$

in which R is the gas constant, and x_i are the molar fractions of the element i. The binary excess term is given by:

$${}^{E}G^{bin,\phi} = \sum_{i=1}^{2} \sum_{j>i}^{3} x_i x_j \sum_{v=0}^{n} L_{ij}^{v,\phi} (x_i - x_j)^v \quad \text{(Eq 4)}$$

This corresponds to a Redlich-Kister/Muggianu type extrapolation from the binary sets where $L_{ij}^{v,\phi}$ is the vth interaction parameter between the elements i and j (i, j = Al, Mg, Sn) in the ϕ phase, which is taken from the binary optimization process.

The liquid phase is described using the associate solution model. Review and description of the associate model can be found elsewhere[15,16]. The Gibbs energy of the liquid phase is described by:

$$G^{L}(T, \{y_i\}) = \sum_{i=1}^{4} y_i \cdot G_i^{0,L}(T) + RT \sum_{i=1}^{4} y_i \ln y_i + \sum_{i=1}^{3} \sum_{j>i}^{4} y_i y_j \sum_{v=0}^{n} L_{i,j}^{v,L} (y_i - y_j)^v \quad \text{(Eq 5)}$$

where y_i is the mole fraction of species i (i = Al, Mg, Sn, Mg_2Sn) in the liquid. G^L refers to one mol of formula of the liquid and the number of moles in the liquid phase results from an internal Gibbs energy minimization. $L_{i,j}^{v,L}$ is the vth interaction parameter between the species i and j (j = Al, Mg, Sn, Mg_2Sn) in the liquid phase. These Redlich-Kister type parameters are also optimized based on the input data. Only the interactions between species (Al, Mg_2Sn) reflect a ternary contribution, all other $L_{i,j}^{v,L}$ parameters are given from the binary edge systems.

The experimental data show that ternary liquidus temperatures are generally higher than the calculated extrapolation from the binary thermodynamic data sets predicts. This indicates that the liquid phase is less stable than predicted and that a positive Gibbs energy term in the liquid phase must be added to the model to raise the liquidus surface of the ternary system.

With the use of the single ternary interaction parameter in the associate model of the liquid phase describing the interaction between the liquid associate species Mg_2Sn and liquid Al, $L_{Al,Mg_2Sn}^{0,Liquid} = +20$ kJ/mol, it was possible to fit the thermodynamic model to all experimental thermal data. It is typical that a positive interaction parameter is necessary along the dominating section between the strong associate Mg_2Sn and Al as discussed later.

Results of the final thermodynamic modeling are summarized in the liquidus projection shown in Fig. 2(a) with a detailed view of the Mg-Al-rich side in Fig. 2(b). The corresponding calculated four-phase invariant reactions and three-phase maxima/critical points involving the liquid phase are listed in Table 4. More results can be seen in all the calculated vertical phase diagram sections presented in the discussion section of this paper, where the quality of the thermodynamic model, in terms of how well the experimental data are represented, is discussed. All thermodynamic

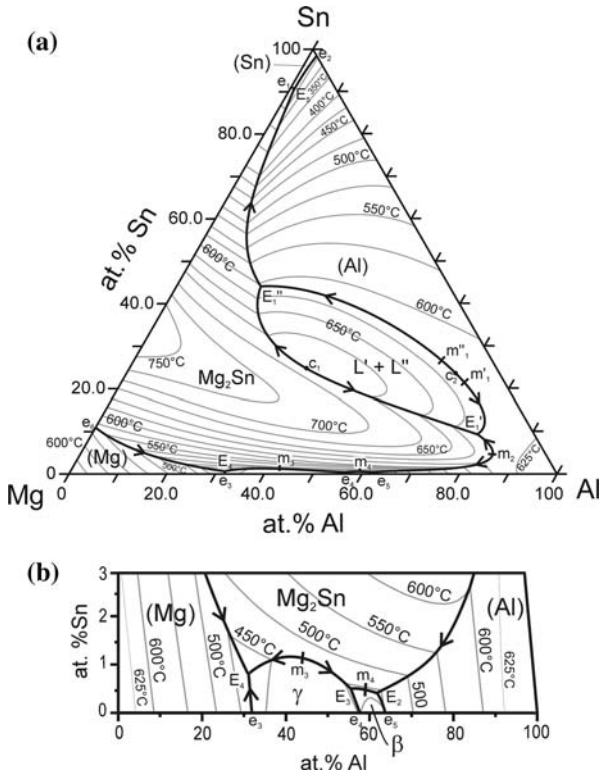

Fig. 2 (a) Calculated Mg-Al-Sn liquidus surface. (b) Magnification of the Mg-Al side of the calculated phase diagram shown in (a)

Table 4 Temperatures and compositions of solution phases at the invariant or critical ternary reactions involving the liquid phase, calculated using the thermodynamic model of the system

Invariant reaction	Type	Calculated temperature, °C	Phase	Composition, at.% Al	Composition, at.% Sn
$\{L' = L''\} \leftrightarrow Mg_2Sn$	c_1-max	690	L′ = L″	36.2	24.9
$L' \leftrightarrow L'' + (Al)$	m_1-max	607.1	L′	69.7	22.0
			L″	63.0	26.9
			(Al)	96.4	0.0
$\{L' = L''\} \leftrightarrow (Al)$	c_2-min	607.05	L′ = L″	67.4	23.7
			(Al)	96.2	0.0
$L \leftrightarrow (Al) + Mg_2Sn$	m_2-max	606.7	L	84.4	4.6
			(Al)	98.2	0.0
$L' \leftrightarrow L'' + (Al) + Mg_2Sn$	E_1	602	L′	79.1	9.3
			L″	17.2	44.2
			(Al)	98.7	0.0
$L \leftrightarrow \gamma + Mg_2Sn$	m_3-max	458	L	45.4	0.8
			γ	46.5	0.0
$L \leftrightarrow \beta + Mg_2Sn$	m_4-max	449	L	59.6	0.5
$L \leftrightarrow (Al) + \beta + Mg_2Sn$	E_2	448	L	62.7	0.4
			(Al)	83.6	0.0
$L \leftrightarrow \beta + \gamma + Mg_2Sn$	E_3	446	L	56.2	0.6
			γ	51.8	0.0
$L \leftrightarrow (Mg) + \gamma + Mg_2Sn$	E_4	431	L	29.4	0.2
			(Mg)	10.6	0.5
			γ	40.0	0.0
$L \leftrightarrow Sn + (Al) + Mg_2Sn$	E_5	202	L	1.0	90.4
			(Al)	100.0	0.0

calculations have been performed using the software package Pandat.[17]

5. Discussion

5.1 Comparison of Solidification Paths of Present Ternary Alloys to Thermodynamic Calculations

The ternary solid-state equilibria are dominated by the Mg_2Sn + (Al) two-phase field. Figures 3 and 4 show the typical morphology of alloys within the two largest solid-state three-phase regions of the Mg-Al-Sn system. While sample 4 is positioned on the magnesium-rich side in the three-phase region Mg_2Sn + (Mg) + γ-$Mg_{17}Al_{12}$ and sample 6 is on the tin-rich side in the Mg_2Sn + (Sn) + (Al) region (Fig. 1), both are positioned on the Mg_2Sn primary crystallization field of the calculated liquidus surface (Fig. 2a) and in fact show a large amount of primary Mg_2Sn. The order of crystallization becomes obvious when analyzing the corresponding calculated *T-x* phase diagram shown in Fig. 5. After primary solidification of Mg_2Sn between 708 and 438 °C, sample 4 goes through a short secondary precipitation of γ-$Mg_{17}Al_{12}$ + Mg_2Sn followed by the eutectic reaction E_4: $L \rightarrow Mg_2Sn + \gamma\text{-}Mg_{17}Al_{12}$ + (Mg). The solidification path of sample 6 starts with the primary Mg_2Sn at 754 °C and, after a transient liquid phase demixing that ends at 602 °C, continues through the phase field L + Mg_2Sn + (Al) before reaching the eutectic reaction E_5: $L \rightarrow Mg_2Sn$ + (Al) + (Sn). For both samples 4 and 6 the occurrence and morphology of the solid phases

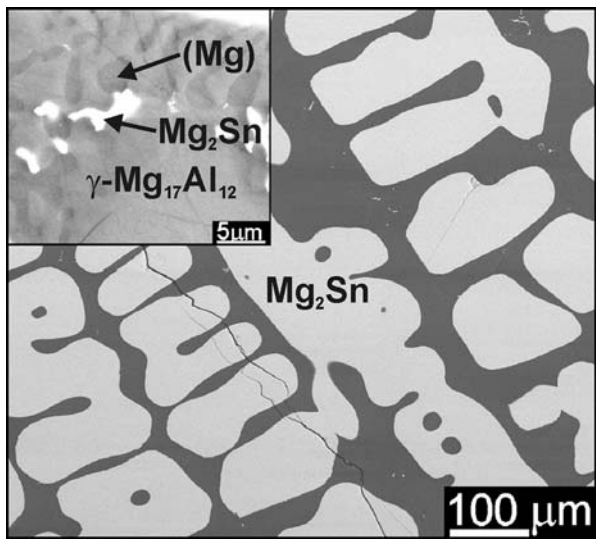

Fig. 3 Scanning electron micrographs of sample 4. The enlargement shows the presence of all three expected phases in the eutectic mixture. All SEM pictures were taken using backscattered electrons to identify the heavier from the lighter phases

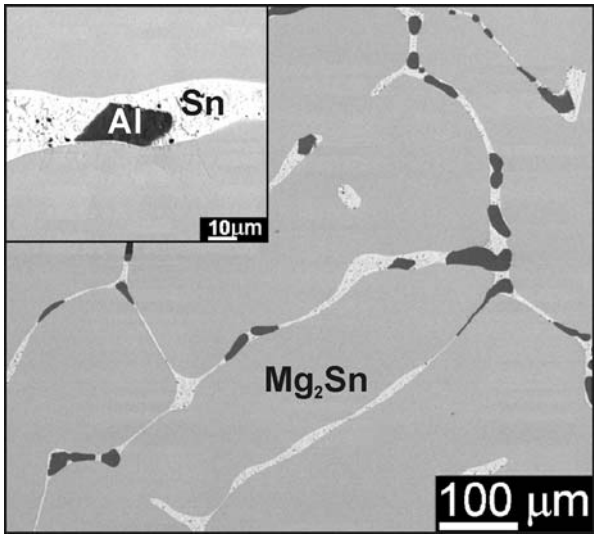

Fig. 4 Scanning electron micrographs of sample 6, in the three-phase region Mg_2Sn-Al-Sn

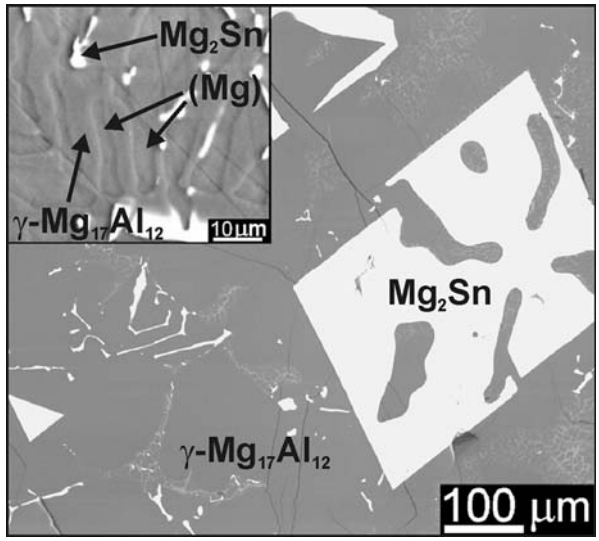

Fig. 6 Scanning electron micrographs of sample 7. The primary Mg_2Sn crystals were slower growing than those in sample 4 (Fig. 3) and therefore show a more typical cubic structure

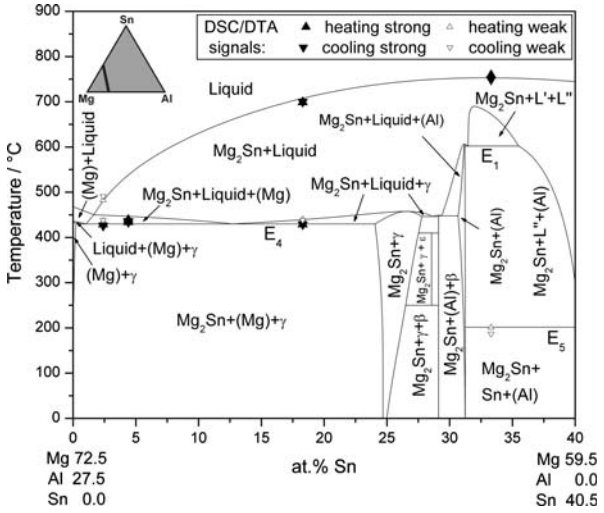

Fig. 5 Calculated vertical section Mg72.5Al27.5-Mg59.5Sn40.5 including the DSC/DTA signals measured in this work from samples 9, 1, 4, and 6

predicted for each of these different solidification steps is reflected in the experimental microstructures.

The rounded shape of the primary Mg_2Sn crystals, in sample 4 (Fig. 3) and sample 6 (Fig. 4), gives the impression of dendritic growth, while a typical cubic crystal shape of the primary Mg_2Sn is seen in samples 7 and 9 (Fig. 6 and 7). This is probably due to a much slower growth rate of the Mg_2Sn crystals in samples 7 and 9. In Fig. 2(a) it can be seen that the solidification path of sample 6, which is positioned very close to Mg_2Sn, crosses a very flat section of the Mg_2Sn liquidus surface. After a temperature drop of 50 °C, which is 10 min in the DTA experiment, over half of the liquid has solidified as Mg_2Sn crystals. During the same time and temperature interval for sample 9, which is positioned further away from Mg_2Sn and on a much steeper section of the liquidus surface, only a very small fraction of the sample has solidified. This slower growth rate of the Mg_2Sn crystals allows enough time for the crystal shape to more properly reflect the cubic crystal structure of Mg_2Sn. It cannot be excluded that the different compositions of the liquids that are in equilibrium with Mg_2Sn also have an impact on the shape of the resulting Mg_2Sn crystals.

A first glance at the SEM pictures of all samples with compositions within the three-phase region Mg_2Sn + (Mg) + γ-$Mg_{17}Al_{12}$ seemed to show only two phases: Mg_2Sn and γ-$Mg_{17}Al_{12}$. A two-phase region this large is impossible knowing that the ternary solubilities are negligible. Thus, the samples were analyzed again. By improving the electrical conductivity of the sample holder material and the contrast settings, photos with a higher resolution could be taken. As a result, the slightly darker (Mg) phase could be distinguished from the γ-$Mg_{17}Al_{12}$ in agreement with the different mass contrast in the backscattered electron images. The (Mg) phase was found to exist in a very fine eutectic structure together with eutectic Mg_2Sn and γ-$Mg_{17}Al_{12}$, which can be seen in the enlargement in Fig. 3, 6, and 7. This is in agreement with the calculated ternary eutectic reaction E_4: $L \rightarrow Mg_2Sn$ + γ-$Mg_{17}Al_{12}$ + (Mg).

Sample 9 is positioned inside an area of the phase diagram that was previously presumed to belong to the liquidus surface of primary magnesium.[6] The micrograph in Fig. 7 clearly shows primary solidification of Mg_2Sn supporting the present thermodynamic calculation of Fig. 5 and 2(a). This proves that the liquidus surface of Mg_2Sn is even larger than assumed in previous work, leaving only a slim primary (Mg) liquidus surface.

In addition to the agreement concerning the solidification paths it is obvious from Fig. 5, 8, and 9 that the thermal analysis results of the present investigation are in very good agreement with the calculated phase diagrams. This is also

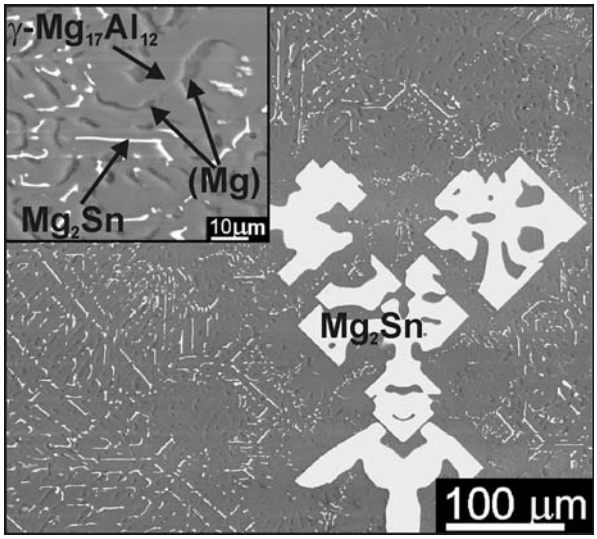

Fig. 7 Scanning electron micrographs of sample 9. This sample, with the lowest at.% Sn shows the highest volume fraction of the (Mg) phase but still features primary Mg_2Sn

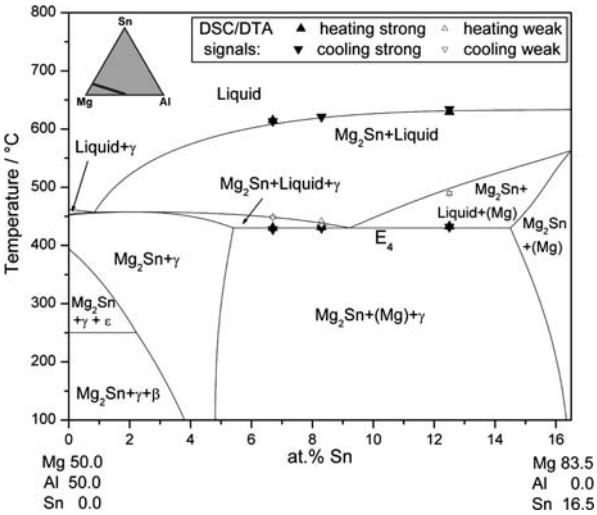

Fig. 8 Calculated vertical section Mg50.0Al50.0-Mg83.5Sn16.5 including the DSC/DTA signals measured in this work from samples 7, 5, and 2

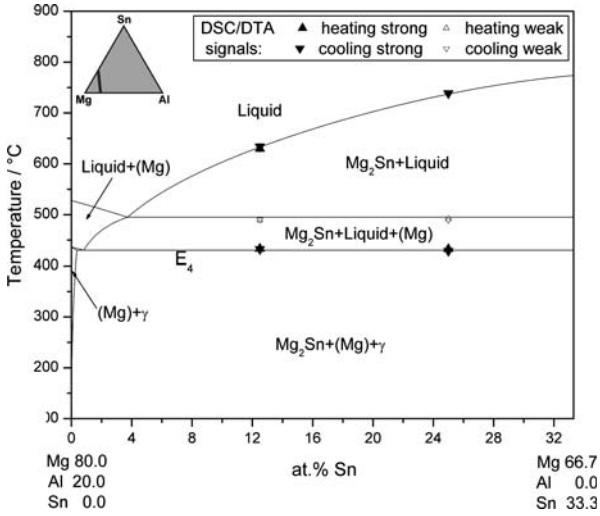

Fig. 9 Calculated vertical section Mg80.0Al20.0-Mg66.7Sn33.3 including the DSC/DTA signals measured in this work from samples 2 and 8

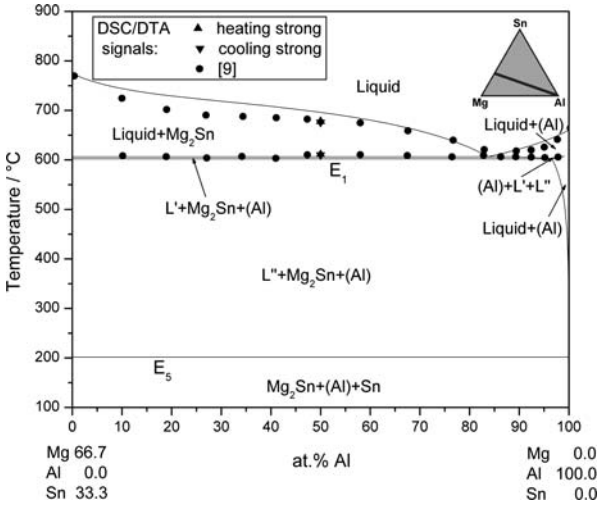

Fig. 10 Calculated vertical section Mg66.7Sn33.3-Al100.0 including DTA signals measured by Badaeva and Kusnetsova[9] and the DSC signals from sample 3 in this work

true for the phase analysis of the samples equilibrated at 400 °C noted in Fig. 1. This provides strong confirmation of the thermodynamic description generated in this work.

5.2 Comparison of Calculated Phase Equilibria to Experimental Literature Data

Pertinent phase equilibrium data from all previous publications were extracted and also used during the modeling stage of this investigation. Only original experimental data were used and reanalyzed without taking into account estimations, explanations, or reviews. The sample compositions used by previous authors are mostly lower in magnesium content than the samples used in the present study. Sample number 3 in this study was chosen on a section previously investigated to scrutinize the accuracy of earlier experimentation. The good correlation can be seen in Fig. 10 where the DSC signals from sample number 3 are plotted together with experimental data from the literature.[9] The reproducibility of the experimental data used to create a thermodynamic model for this ternary system is demonstrated again in Fig. 11 where two authors[8,10] have conducted thermal analysis along the same section in the ternary phase diagram. Further literature data[9] can be seen in Fig. 12 and 13, which are well reflected by the simple thermodynamic model. In fact, the representation of all invariant reactions in the ternary system is very good. While the experimental liquidus surface data from this work are

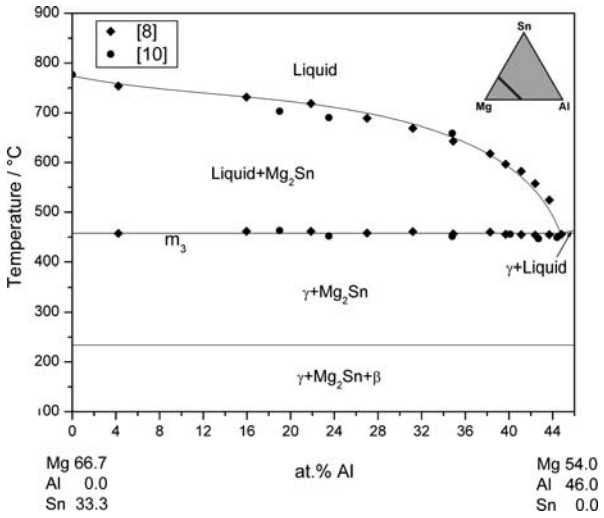

Fig. 11 Calculated vertical section Mg66.7Sn33.3-Mg54.0Al 46.0 including the DTA signals measured in Ref. 8 and 10

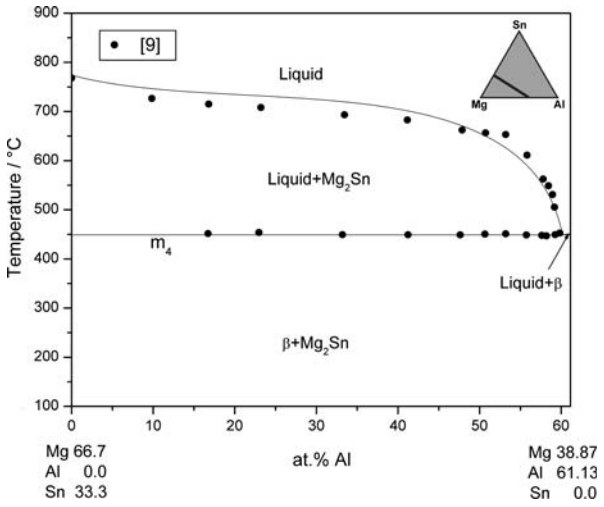

Fig. 12 Calculated vertical section Mg66.7Sn33.3-Mg38.87Al61.13 including the DTA signals measured by Badaeva and Kusnetsova[9]

represented very accurately, a deviation from the liquidus temperatures, as measured by Badaeva and Kusnetsova[9] in the tin-poor section of the system, can be seen in Fig. 10 and 12. The greatest deviations in the liquidus temperature can be seen around 10 to 50 at.% Al in Fig. 10; however, this is accepted in exchange for the accurate description of the qualitative change in primary crystallization fields between 80 and 90 at.% Al. An attempt to obtain a closer fit to such details without losing the very good overall agreement with the experimental data proved difficult. It was finally decided not to sacrifice the simplicity of the model with a single, constant ternary interaction term.

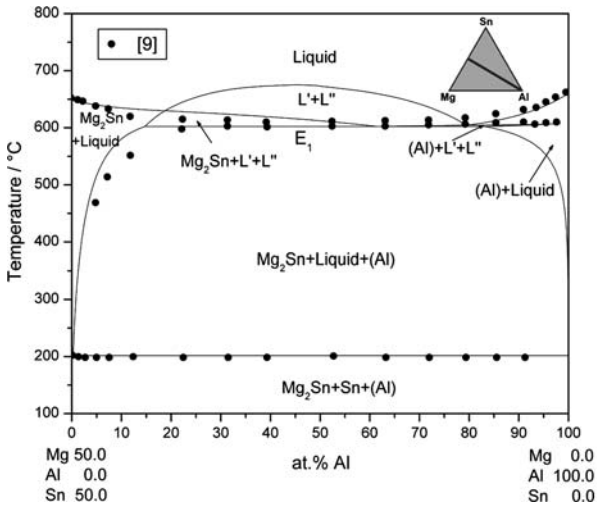

Fig. 13 Calculated vertical section Mg50.0Sn50.0-Al100.0 including the DTA signals measured by Badaeva and Kusnetsova[9]

The thermodynamic model predicts a miscibility gap in the liquid phase in the center of the system, which was not considered in previous work.[5,6] This can be seen in the *T*-*x* sections shown in Fig. 13 and 5 and on the liquidus surface in Fig. 2(a). Thermal data[9] show an unmistakable horizontal array (Fig. 13) that proves that this stable liquid miscibility gap does exist in the in the ternary Mg-Al-Sn system and is not an artefact produced by the thermodynamic model. It also shows that the corresponding invariant reaction E_1, produced by the intersection of the liquid gap with the primary crystallization fields of Mg_2Sn and (Al) and calculated at 602 °C, is in perfect agreement with the experimental data in Fig. 13. The shape of the experimental liquidus line data in Fig. 10 to 12 also supports this conclusion. These sections are close to, but not cutting through, the stable liquid gap. However, the broad and S-shaped liquidus lines of Mg_2Sn are strong evidence for the occurrence of a tendency for demixing with a metastable liquid gap just covered by the stable primary crystallization of Mg_2Sn. This metastable liquid miscibility gap also extends into the Al-Sn binary system,[1] where it occurs with a critical point at 22 at.% Sn and 535 °C, covered by the stable liquidus line of (Al).

It is worth discussing why and to what extent a ternary liquid miscibility gap occurs in this system. Typically, a moderate liquid miscibility gap occurs along a ternary section between a composition of strong short-range order in one binary system and the third component. This is also why a positive interaction parameter is necessary along that dominating section between the strong associate Mg_2Sn and Al as given in the present model with $L^{0,\mathrm{Liquid}}_{\mathrm{Al,Mg_2Sn}} = +20$ kJ/mol. This is because of the use of the associate solution model in the binary Mg-Sn system and for the extrapolation into the ternary system with Eq 5. If a zero value of $L^{0,\mathrm{Liquid}}_{\mathrm{Al,Mg_2Sn}}$ is assumed, this equation generates an essentially ideal solution along the Mg_2Sn-Al section where the species fractions y_{Mg} and y_{Sn} are very small. In that case

not even a small tendency for demixing would have been predicted, and a simple deep eutectic around 550 °C would have appeared in Fig. 10, in conflict with the experimental data. The proper thermodynamic description generates two narrowly spaced horizontal lines; the upper one at 606 °C marks the start of the (Al) crystallization from the Al-rich liquid L′ in the L′ + Mg_2Sn + (Al) phase field. The lower one at 602 °C is the truly invariant four-phase reaction E_1, where the Al-rich liquid L′ decomposes into the Al-poor liquid L″ + Mg_2Sn + (Al).

5.3 Comparison of Calculated Thermodynamic Data to Experimental Literature Data

The experimental enthalpy of mixing in ternary liquid alloys, measured by Sommer et al.,[7] has not been used for the thermodynamic optimization, but is compared below with the present calculations as a final check on the consistency of the modeling. It is noted that the experiments had been performed at 735 and 835 °C,[7] which is above the liquid miscibility gap shown in Fig. 2(a), and thus no complications due to demixing are expected. These experiments involved small incremental additions of the third component to a binary liquid alloy at constant temperature in the calorimeter, and therefore the change in the enthalpy of mixing, $\delta\Delta H$, has been measured. To correctly compare the experimental results presented by Sommer et al.[7] with enthalpy of mixing values calculated using the present model, Sommer's tabulated results were used rather than the presented diagrams.[7] These tabulated $\delta\Delta H$ values represent the integral enthalpy of mixing for a hypothetical binary alloy with the third element (e.g., Mg_2Sn with Al, Fig. 14). These values are then added to a reference state line, which uses an assumed value for the mixing enthalpy of the binary starting alloy and for the pure Al or Sn (which is of course zero for the chosen reference state of pure liquid elements) to give the integral enthalpy of mixing, ΔH, of the components Al, Mg, and Sn. The ΔH values labeled "[7]" in Fig. 14 to 17 are generated by adding Sommer's tabulated $\delta\Delta H$ values to a reference state line that uses the current accepted binary enthalpy of mixing values rather than those used in Sommer et al.[7] (e.g., 14.24 kJ/mol rather than −14.8 kJ/mol, Fig. 14). This procedure and the exact definition of $\delta\Delta H$ was confirmed by Sommer.[18]

Figures 15 and 16 show a near to perfect fit between the calculated and experimental enthalpy of mixing values, well within even the experimental uncertainty, which is given[7] as ±5.5%. Figure 14 shows the greatest deviation between 20 and 60 at.% Al. Interestingly, this correlates with the region in Fig. 10 where the liquidus temperature calculated using the thermodynamic model deviates the most from the experimental values from Badaeva and Kusnetsova.[9] It was possible to model the enthalpy data in Fig. 14 using a single L^0 parameter of +30 kJ/mol rather than +20 kJ/mol. However, this approach does not allow the invariant reactions in the isopleth sections to be modeled well.

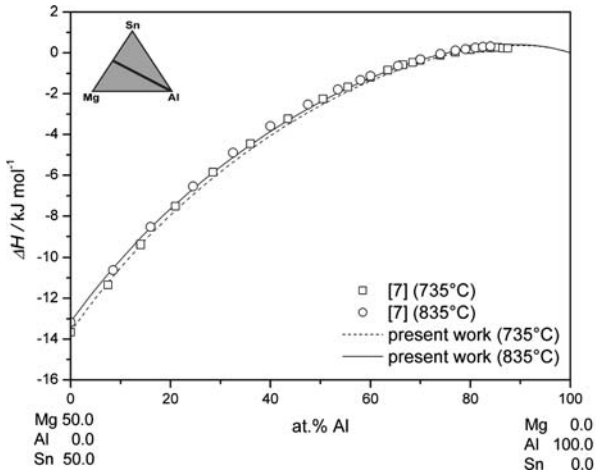

Fig. 15 The enthalpy of mixing of liquid Mg-Al-Sn alloys along section Mg50.0Sn50.0-Al at 835 and 735 °C calculated in this work compared with experimental data[7]

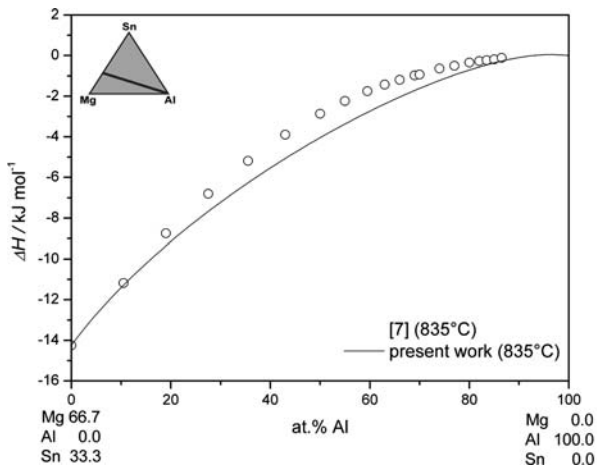

Fig. 14 The enthalpy of mixing of liquid Mg-Al-Sn alloys along section Mg66.7Sn33.3-Al at 835 °C calculated in this work compared with experimental data[7]

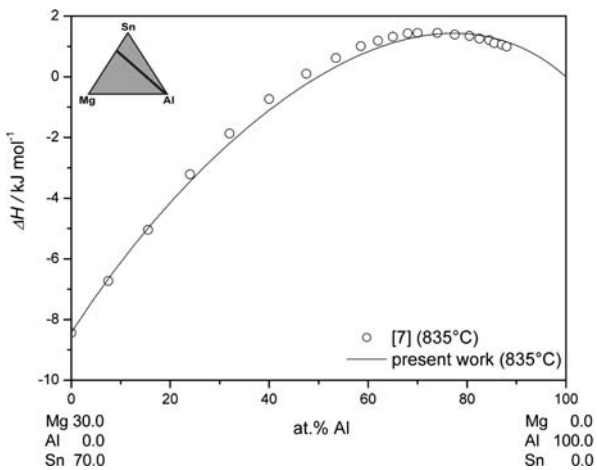

Fig. 16 The enthalpy of mixing of liquid Mg-Al-Sn alloys along section Mg30.0Sn70.0-Al at 835 °C calculated in this work compared with experimental data[7]

The section Mg50.0Al50.0-Sn shown in Fig. 17 intersects the three sections already mentioned; even though the difference between experimental and calculated ΔH values shows quite a different pattern, especially when compared with Fig. 15 and 16. It should be noted that a similar pattern is observed between the experimental data on that section Mg50.0Al50.0-Sn and the thermodynamic model proposed by Sommer et al.[7] to describe just these enthalpy data without attempting to also describe the entire phase diagram using the same model.

Overall, the enthalpy of mixing curves calculated using the current thermodynamic model correlate very well with the experimental values from the literature. This additional check of the model consistency is successful.

5.4 Special Features of the Ternary Liquid Miscibility Gap

The liquid miscibility gap shown in the calculated liquidus surface in Fig. 2(a) exhibits a number of features that deserve to be explained a little more closely. First of all, the liquid gap is not stable along the exact section Mg_2Sn-Al, as also seen from Fig. 10. It is more pronounced toward the Al-Sn edge binary with a summit close to the critical point c_1 and slightly above 690 °C.

As detailed previously, the main reason for the stability of this miscibility gap in the ternary is the extremely high thermodynamic stability of the liquid phase around the Mg_2Sn composition, caused by strong short-range order. If both the Mg-Al and Mg-Sn liquid alloys were to display close to ideal mixing behavior, a hypothetical and more symmetrical case, the summit of the ternary miscibility gap would be right on the Mg_2Sn-Al section and the maximum critical point c_1 would shift toward the Mg-Al side and become a minimum. In reality, the Mg-Sn liquid alloys show a substantial positive deviation from ideal mixing, whereas the Mg-Al liquid phase is roughly ideal with only a slight negative deviation around 700 °C. This is the reason why the summit of the ternary liquid miscibility gap is shifted away from the Mg_2Sn-Al section toward the Al-Sn edge binary.

In addition to the maximum critical point (c_1-max = 690 °C) on the Mg_2Sn side, the ternary miscibility gap features a minimum critical point (c_2-min = 607.05 °C) on the (Al) side. At both of these critical points, denoted with c, the two liquid compositions L' and L'' fall together. This means that the three-phase triangles (c_1: $Mg_2Sn + L' + L''$ and c_2: (Al) + $L' + L''$) degenerate to a line, because one side length is reduced to zero. The equilibrium reactions are given in Table 4. The miscibility gap also features a double maximum, denoted with m_1. At 607.1 C the three-phase triangle (Al) + $L' + L''$ degenerates to a line with three non-zero sides as shown in Fig. 18. This reaction is denoted with m because it is the same type of degeneration as m_2, m_3, and m_4. The only difference is that two of the three phases are liquid, denoted as m_1' and m_1'' in Fig. 2(a). Below the four-phase invariant reaction (E_1 = 602 °C) no stable two-phase equilibrium $L' + L''$ exists. The label E_1 is chosen since this "monotectic" reaction is of the eutectic decomposition type.

The particular region in Fig. 2(a) around the double maximum m_1 and the minimum c_2 needs explanation. A schematic diagram showing the development of the tie-triangles (Al) + $L' + L''$ between the temperatures of m_1 and c_2 is presented in Fig. 18. It is important to note that at c_2 the curvature of the monovariant line of the liquidus surface, shown dashed, is exaggerated. The composition of the (Al) solid-solution phase is also stretched to clarify the point. At m_1 = 607.1 °C, the three-phase triangle (Al) + $L' + L''$ degenerates to a single line and the reaction $L' \leftrightarrow L'' +$ (Al) must become invariant. These two distinct liquid compositions are denoted as m_1' and m_1'' in Fig. 2(a). Either side of m_1' and m_1'' the three-phase equilibrium $L' + L'' +$ (Al) becomes monovariant and occurs at lower temperatures.

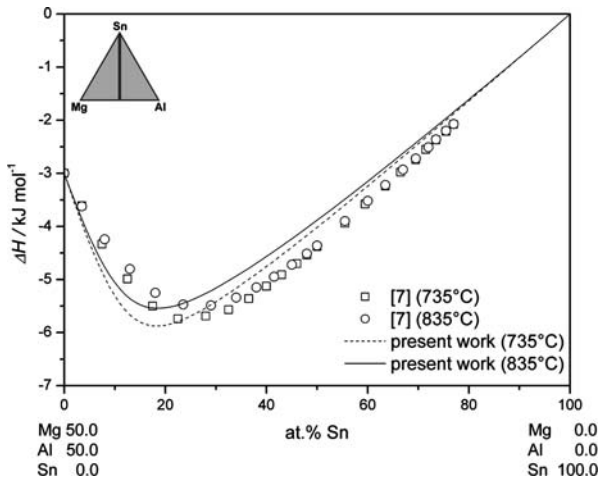

Fig. 17 The enthalpy of mixing of liquid Mg-Al-Sn alloys along section Mg50.0Al50.0-Sn at 835 and 735 °C calculated in this work compared with experimental data[7]

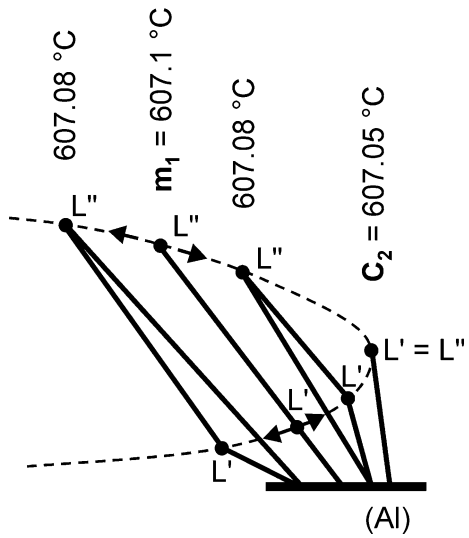

Fig. 18 Development of the tie triangles L′ + L″ + (Al) around the reactions m_1-max and c_2-min. The dashed line is an exaggerated part of the monovariant line of the liquidus surface, ending in the points E_1' and E_1'' of Fig. 2(a)

This implies the opening of the three-phase field to actual triangles, as depicted with the two triangles at an intermediate temperature of 607.08 °C in Fig. 18. While the left triangle moves toward E_1 with lower temperature, the right triangle moves toward the minimum critical point c_2. Here, at the minimum temperature of 607.05 °C, the compositions of L' and L'' become equal and the triangle $L' + L'' + (Al)$ reduces to a tie line $\{L' = L''\} + (Al)$.

This particular form of liquid miscibility gap with a minimum critical point and neighboring maxima very close in temperature and composition has not come to our attention in any other system. The thorough examination of these complex phase relations is quite interesting from the academic point of view of heterogeneous phase equilibria. It is possible that the real liquid miscibility gap in the Mg-Al-Sn system features such a combination of minimum critical point and neighboring maxima since the perfect consistency with all rules of heterogeneous phase equilibria were elaborated. However, as these points are calculated by the thermodynamic model less than 1° apart, it would only take a very small change in the Gibbs energy of the phases to alter the shape of the liquidus surface slightly, and thus the form and tie-line directions of the miscibility gap, to produce another possible variant. In this variant the degeneracy of the tie triangle to a line does not occur, thus removing the invariant reaction m_1 and letting this monovariant three-phase equilibrium terminate at a *maximum* critical point c_2, where it again shrinks to a tie line $\{L' = L''\} + (Al)$. For practical applications, it is enough to state that the liquidus surface of (Al) and its intersection with the liquid miscibility gap around the region of m_1', c_2, and m_1'' in Fig. 2(a) is extremely flat.

6. Conclusion

- A consistent thermodynamic description of the Mg-Al-Sn alloy system was developed for the first time based on the authors' key experiments in the Mg-rich corner of the system and all available phase equilibrium data from the literature.
- By using just one simple ternary parameter describing the interaction along the dominating section of the associate solution model in the liquid phase ($L^{0,\text{Liquid}}_{\text{Al,Mg}_2\text{Sn}} = +20$ kJ/mol), it was possible to calculate phase diagrams that represent all invariant reactions very closely and also match the experimental liquidus data very closely in most sections of the ternary system.
- The phase sequence and morphology in the microstructure of slowly solidified phases are clearly supporting the solidification paths of Mg-rich alloys obtained by thermodynamic equilibrium calculations based on the new model of the ternary system.
- Good correlation between calculated enthalpy of mixing curves and the measured values from Sommer et al.[7] provides a successful additional check of the consistency of the thermodynamic description developed during the present study that was not optimized using these thermodynamic data.
- A ternary liquid miscibility gap is detected in the Mg-Al-Sn phase diagram that produces intricate details.
- The thermodynamic model presented here is considered to be a sound basis for higher-order modeling of multicomponent Mg alloys.

Acknowledgment

This study is supported by the German Research Foundation (DFG) in the Priority Programme "DFG-SPP 1168: InnoMagTec" under Grant No. Schm 588/26.

References

1. S. Fries and H.L. Lukas, System Al-Sn, in COST507, *Definition of Thermochemical and Thermophysical Properties to Provide a Database for the Development of New Light Alloys, Vol 2, Thermochemical Database for Light Metal Alloys*, I. Ansara, A.T. Dinsdale, and M.H. Rand, Eds., European Communities, 1998, p 81-82
2. S.G. Fries and H.L. Lukas, Optimisation of the Mg-Sn System, *J Chem. Phys.*, 1993, **90**, p 181-187
3. S. Fries, private communication 2004
4. P. Liang, H.-L. Su, P. Donnadieu, M.G. Harmelin, A. Quivy, P. Ochin, G. Effenberg, H.J. Seifert, H.L. Lukas, and F. Aldinger, Experimental Investigation and Thermodynamic Calculation of the Central Part of the Mg-Al Phase Diagram, *Z. Metallkde.*, 1998, **89**(8), p 536-540
5. G.V. Raynor, Constitution of Ternary and Some More Complex Alloys of Magnesium, *Int. Met. Rev.*, 1977, June, p 65-96
6. L. Rokhlin and H.L. Lukas, Aluminium-Magnesium-Tin, *Landolt-Boernstein, Numerical Data and Functional Relationships in Science and Technology (New Series). Group IV: Physical Chemistry.* W. Martiensen, Ed., Ternary Alloy Systems. Phase Diagrams, Crystallographic and Thermodynamic Data, Vol 11 (A3), G. Effenberg and S. Ilyenko, Eds., Springer-Verlag, 2005, p 178-186
7. F. Sommer, N. Rupf-Bolz, and B. Predel, Untersuchungen zur Temperaturabhängigkeit der Mischungsenthalpie ternärer Legierungsschmelzen, *Z. Metallkde.*, 1983, **74**, p 165-171, in German
8. "Liquidus Determinations of Polynary Magnesium Alloys," Final Status Report No. 15004, DowChemicals, Office of Naval Res., Contract No. N9 ONR 85900, 1950, **2**, p 1-20
9. T.A. Badaeva and R.I. Kusnetsova, The Structure of Alloys of Aluminium with Magnesium and Tin, *Tr. Inst. Metall.*, 1958, **3**, p 203-215
10. E.M. Semenova, Equilibrium Diagram of the Mg-Al-Sn System in the Magnesium-Rich Region, *Dokl. Akad.*, 1969, **188**, p 1308-1310, in Russian
11. D. Mirković and R. Schmid-Fetzer, Solidification Curves for Commercial Mg Alloys Obtained from Heat Transfer Modelled DTA Experiments, *Z. Metallkde.*, 2006, **97**, p 119-129
12. W. Kraus and G. Nolze, PowderCell for Windows version 2.4, Federal Institute for Materials Research and Testing, Berlin, Germany, http://www.bam.de/de/service/publikationen/powder_cell.htm
13. P. Villars and L.D. Clavert, *Pearson's Handbook of Crystallographic Data for Intermetallic Phases*, 2nd ed., ASM International, 1991

14. A.T. Dinsdale, SGTE data for pure elements, *Calphad*, 1991, **15**, p 317-425
15. F. Sommer, Association Model for the Description of the Thermodynamic Functions of Liquid Alloys, *Z. Metallkde.*, 1982, **73**, p 72-76
16. R. Schmid and Y.A. Chang, A Thermodynamic Study on an Associated Solution Model for Liquid Alloys, *Calphad*, 1985, **9**(4), p 363-382
17. S.-L. Chen, S. Daniel, F. Zhang, Y.A. Chang, X.-Y. Yan, F.-Y. Xie, R. Schmid-Fetzer, and W.A. Oates, The Pandat Software Package and its Applications, *Calphad*, 2002, **26**, p 175-188
18. F. Sommer, private communication, 2006
19. T.B. Massalski, H. Okamoto, P.R. Subramanian, and L. Kacprzak, Eds., *Binary Alloy Phase Diagrams*, 2nd ed., ASM International, 1990
20. W. Hume-Rothery and G.V. Raynor, On the Nature of Intermetallic Compounds of the Type Mg_2Sn, *Philos. Mag. S.7*, 1938, **25**, p 335-339
21. H. Westlinning and W. Klemm, Die Löslichkeit von Mg_2Si, Mg_2Ge, Mg_2Sn und Mg_2Pb in Aluminium, *Z. Elektrochem.*, 1943, **40**(4&5), p 198-200, in German
22. Ch.V. Kopetsky and E.M. Semenova, Investigations of the Equilibrium Diagram of the Mg-Al-Sn System in the Magnesium-Rich Region, *Tsvetn. Metall.*, 1968, **5**, p 78-82, in Russian
23. E.M. Semenova, Phase Composition and Properties of Alloys of the Mg-Al-Sn System. *Tr. Inst. Metall.*, 1973, p 165-168 (in Russian)
24. A.L. Bowles, C. Balwert, N. Hort, and K.U. Kainer, Microstructural Investigations of the Mg-Sn and Mg-Sn-Al Alloy Systems. *Magnesium Technol.*, 2004, p 307-310